EFDA–JET–PR(08)45

J. Rapp, Y. Corre, Y. Andrew, M.R. de Baar, M. Beurskens, S. Brezinsek, M. Brix, S. Devaux, T. Eich, R. Felton, W. Fundamenski, C. Giroud, D. Howell, A. Huber, S. Jachmich, E. Joffrin, A. Korotkov, G.F. Matthews, D.C. McDonald, A. Meigs, P. Monier-Garbet, P. Morgan, I. Nunes, G.J. van Rooij, O. Sauter, M.F. Stamp, G. Telesca, P.C. de Vries, R. Zagorski and JET EFDA contributors

Integrated Scenario with Type-III ELMy H-mode Edge: Extrapolation to ITER

Integrated Scenario with Type-III ELMy H-mode Edge: Extrapolation to ITER

J. Rapp[1,2], Y. Corre[3], Y. Andrew[4], M.R. de Baar[1], M. Beurskens[4], S. Brezinsek[2], M. Brix[2], S. Devaux[5], T. Eich[5], R. Felton[4], W. Fundamenski[4], C. Giroud[4], D. Howell[4], A. Huber[2], S. Jachmich[6], E. Joffrin[3], A. Korotkov[4], G.F. Matthews[4], D.C. McDonald[4], A. Meigs[4], P. Monier-Garbet[3], P. Morgan[4], I. Nunes[7], G.J. van Rooij[1], O. Sauter[8], M.F. Stamp[4], G. Telesca[6], P.C. de Vries[4], R. Zagorski[9] and JET EFDA contributors*

JET-EFDA, Culham Science Centre, OX14 3DB, Abingdon, UK

[1]FOM Instituut voor Plasma Fysica Rijnhuizen, EURATOM Association, TEC, Nieuwegein, The Netherlands.
[2]IEF-4, Forschungszentrum Jülich GmbH, EURATOM Association, TEC, Jülich, Germany.
[3]Association EURATOM-CEA sur la Fusion Controlee, Cadarache, Saint-Paul-lez-Durance, France.
[4] EURATOM-UKAEA Fusion Association, Culham Science Centre, OX14 3DB, Abingdon, OXON, UK
[5] Max-Planck Institut für Plasmaphysik, EURATOM Association, Garching, Germany.
[6]LPP-ERM/KMS, EURATOM-Belgian State Association, TEC, Brussels, Belgium.
[7] Association EURATOM/IST, Centro de Fusao Nuclear, Lisbon, Portugal.
[8] CRPP, Association EURATOM-Confederation Suisse, EPFL, Lausanne, Switzerland.
[9]Institute of Plasma Physics and Laser Microfusion, EURATOM Association, Warsaw, Poland.
** See annex of F. Romanelli et al, "Overview of JET Results",*
(Proc. 22 [nd] IAEA Fusion Energy Conference, Geneva, Switzerland (2008)).

Preprint of Paper to be submitted for publication in
Fusion Engineering ans Design

ABSTRACT.

One of the most severe problems for fusion reactors is the power load on the plasma facing components. The challenge is to develop operation scenarios, which combine sufficient energy confinement with benign heat loads to the plasma facing components. The radiative type-III ELMy H-mode seems a possible solution for such an integrated ITER scenario. Most notably the transient heat loads due to type-III ELMs are acceptable with even the most stringent boundary conditions. For instance, on JET the transient heat loads due to type-III ELMs onto the outer divertor target were reduced to 2kJ per square meter. Scaled to ITER, type-III ELMy H-modes are expected to have a power load of approximately 0.3MJ per square meter transiently. This was achieved in experiments carried out with nitrogen seeding to mitigate the transient and steady state heat flux to the divertor. Typically the confinement is reduced by about 8-20% compared to the type-I ELMy H-mode base scenario. However, increasing the plasma current to 17MA on ITER and hence reducing the edge safety factor to 2.6, would allow Q=10 operation at a reduced confinement enhancement factor. This operation scenario was demonstrated at JET up to plasma currents of 3.25MA. At the highest plasma current the effective charge Zeff can be as low as 1.4, mainly due to the increased absolute density and reduced carbon erosion. A large database of highly radiative type-III ELMy H-modes on JET is used for extrapolations to ITER. The data set shows no apparent dependence of the confinement enhancement factor on collisionality. The scaling of the confinement time with respect to the ion gyro radius is close to gyro-Bohm scaling. The 'hybrid' regime, designed for high beta stationary scenarios, has been extended recently at JET to the type-III ELMy H-mode operation by nitrogen seeding (at a plasma current of 1.7MA) up to a normalized pressure (beta) of 2.6. Similar to the standard ELMy H-mode the confinement enhancement factor is reduced by about 20%. The 'hybrid' type-III ELMy Hmode scenario shows improved edge plasma condition without significant modification of the q-profile (stabilized near unity in the plasma core in order to reduce the sawteeth activity), indicating it is compatible with high beta operation (optimized for current drive sources). Extrapolations to ITER are done with an integrated core/edge model.

1. INTRODUCTION

One of the most severe problems for fusion reactors is the power load on the plasma facing components. Technically only loads of less than 10 MW/m^2 in steady state and less than 0.5 MJ/m2 [1] during transients, caused by so-called Edge Localized Modes (ELMs) [2], which are an integral part of the H-mode [3], are acceptable. This effectively means that the unmitigated type-I ELMy H-mode is not acceptable for ITER. The challenge is to develop alternative scenarios, which combine sufficient energy confinement to achieve fusion power amplification factors of Q=10, with benign heat loads to the plasma facing components. The radiative type-III ELMy H-mode seems a possible solution for such an integrated ITER scenario. Most notably the transient heat loads due to type-III ELMs are acceptable with even the most stringent boundary conditions. This was achieved in experiments carried out with nitrogen seeding to mitigate the transient and steady state heat flux to

the divertor. Typically the confinement is reduced by 8-20% compared to the type-I ELMy H-mode baseline scenario. The reduction in stored energy can be regained by either (a) increasing the plasma current or (b) increasing the plasma core confinement. Both routes have been investigated at JET with the standard ELMy H-mode and the so-called Hybrid scenario.

2. HIGHLY RADIATIVE SCENARIOS WITH TYPE-III ELMY EDGE

2.1. STANDARD HIGHLY RADIATIVE NITROGEN SEEDED ELMY H-MODE WITH TYPE-III ELMS

Increasing the plasma current to I_p = 17MA on ITER and hence reducing the edge safety factor q_{95} to 2.6, would allow Q = 10 operation at a confinement enhancement factor of $H_{98(y,2)} = 0.75$ [4] at a high density of 100% the Greenwald density [5] ($\bar{n}_e / n^{GW} = N^{GW} = 1$). The target values for this ITER operation scenario are $\nu^* = 0.042$, $\rho^* = 0.0015$, $N^{GW} = 1$, $Z_{eff} \leq 1.7$, $\bar{n}_e = 13.4 \times 10^{19}$ m^{-3}, W_{th} = 325MJ, $W_{ped} = 0.35 \times W_{th}$, T_{ped} = 2keV and $f_{rad} = 0.75$. This operation scenario was demonstrated at JET in a standard inductive scenario. To obtain these high densities high triangularity plasma configurations had to be chosen. All normalized parameters, including confinement $H_{98(y,2)}$, density N^{GW}, normalized pressure β_N, radiative power fraction f_{rad}, plasma effective charge Z_{eff} were met simultaneously [6]. In recent JET campaigns this plasma regime has been extended to plasma currents of 3.25MA. In those high current discharges central line averaged densities of up 12×10^{19} m^{-3} were reached. Figure 1 shows an overview of such a discharge. The plasma are heated with Neutral Beam Injection (NBI) and Ion Cyclotron Resonance Heating (ICRH).

2.2. HYBRID SCENARIO WITH NITROGEN SEEDING AND TYPE-III ELMS

An integrated hybrid type-III ELM regime with $\beta_N^{therm} = 2.2$ ($P_{NBI} \approx 20-22$MW) and $H_{98(y,2)} \approx 0.83$ has been successfully developed on JET with nitrogen seeding (see overview fig.2). The target plasma scenario is a hybrid H-mode [7] (defined here as an optimized scenario for high $\bar{N}$ operation with moderate MHD activity) with type-I ELMs (Pulse No: 68505), where pedestal plasma temperature is T_{ped} = 1keV, I_p = 1.7MA, toroidal magnetic field B_t = 1.7T, $\bar{n}_e \approx 5 \times 10^{19}$ m^{-3} (70% of the Greenwald density), $q_{95} \approx 3.2$ in which injected neutral beam power (NBI) is feed-back controlled to $\approx 14-16$MW to achieve a β_N of 3 (non-thermal β_N). The thermal confinement enhancement factor achieved in the target plasma scenario is $H_{98(y,2)} \approx 1.05$ and the plasma effective charge is Z_{eff} = 1.8. A high triangularity magnetic configuration ($\delta = 0.44$) is used. Lower hybrid heating is used during the plasma current ramp up (for a duration of about 3s) to delay the plasma current profile penetration with the aim of producing a broad q-profile when the main heating is applied. This is followed by an intermediate β_N = 2 phase (for a duration of 3s) for stabilization of the q-profile close to 1 in order to minimize the impact of sawtooth on stability. The β_N request is then increased and kept constant during 4 seconds. During this phase, a pre-set injection of deuterium is applied: β_N = 3 has been obtained with low deuterium fuelling (Pulse No: 68505: $\Gamma_D = 0.6 \times 10^{22}$ electrons per second) and $\beta_N^{therm} = 2.2$ with high deuterium fuelling and density close to the Greenwald density

$\bar{n}_e = 0.95 \leq n_e^{GW}$ (Pulse No: 68515: $\Gamma_D = 5 \times 10^{22}$ el/s). Nitrogen injection is applied in addition to deuterium fuelling during the first three seconds of the high β_N plateau (when $\beta_N^{therm} = 2.2$). Deuterium is injected in the bottom of the divertor near the outer strike point on the Low Field Side (LFS) while nitrogen is injected into the private-flux region from the horizontal target plate located on the High Field Side (HFS). The maximum radiated power fraction achieved with deuterium fuelling alone (with mainly D and C radiators) is $P_{rad}/P_{heat} = 0.45$ with density close to the Greenwald limit $\bar{n}_e \approx n^{GW}$ (Pulse No: 68739). Using deuterium plus nitrogen fuelling enables to increase the radiative fraction (with mainly D, C and N radiators), 70% has been achieved during the experiment. The type III ELM regime is achieved here when $P_{rad}/P_{heat} \geq 0.55$ and the pedestal ion temperature T_{ped} is reduced to values below 750eV. The degradation of global confinement associated with the type-III ELM regime is about 10% compared to the reference hybrid high D-fuelling discharge (Pulse No: 68515), which uses the same D-fuelling: $\Gamma_D = 5 \times 10^{22}$ el/s.

3. POWER LOAD TO THE PLASMA FACING COMPONENTS

It has been found that the power load to the divertor can be reduced significantly in the nitrogen seeded type-III ELMy H-mode. In steady state radiative power fraction of 97% were already achieved [6]. Furthermore it should be noted that the transient heat loads due to type-III ELMs can be reduced significantly in type-III ELMs [8, 9]. For instance, on JET the transient heat loads due to type-III ELMs onto the outer divertor target were reduced to 2kJ/m^2 [8]. With the new infrared diagnostic capabilities [10] better measurements with improved time resolution are possible. For the highly radiative nitrogen seeded plasmas the temperature excursions in the outer divertor due to the type-III ELMs is only in the range of 10^{o}C. This corresponds to a power flux density of about 1 MW/m2. At the inner divertor it is typically half of that value. No difference between the standard type-III ELMy H-mode and the hybrid type-III ELMy H-mode was observed. The divertor heat load due to the type-III ELMs normalized to the total stored energy versus the core collisionality is shown in figure 1. The data set shows no apparent dependence of the ELM energy deposition in the divertor as a function of collisionality. If at all the ELM energy loss is slightly decreasing with decreasing collisionality. The absolute value is about 0.1%. Taking a constant W_{div}/W of 0.1% for type-III ELMs in a radiating scenario the ITER divertor load would be about 0.3 MJ. This would approximately translate into 0.1MJ/m^2. However, if a collisionality dependence of W_{div}/W similar to type-I ELMs is assumed, then the energy load to the divertor could be a factor of 3 higher, leading to a predicted energy load of 0.3MJ/m^2. It appears that the ELM rise time for type-III ELMs is much slower than for type-I ELMs. Details of the temporal evolution and spatial energy distribution could influence the predictions and need to further investigated. Even more difficult to predict is the ELM frequency of the radiative type-III ELMs. At JET the ELM frequencies vary between 150Hz and 1kHz.

4. CONFINEMENT SCALING

The main drawback of the type-III ELMy H-mode is it's reduced confinement, when compared to

the type-I ELMy H-mode. The JET steady-state database contains about 576 type-III ELMy H modes and 672 type-I ELMy H-modes. The fit gives a $H_{98(y,2)}$ of 0.95 for the type-I ELMy H-modes and a $H_{98(y,2)}$ of 0.87 for the type-III ELMy H-modes [11]. The parametric dependence in the scaling is otherwise the same for type-I ELMy H-modes and type-III ELMy H-modes. However, for strongly radiating type-III ELMy H-modes the confinement appears to be slightly lower. To investigate this further, a large database of highly radiative type-III ELMy H-modes on JET has been set up, including discharges in low triangularity (lower density) [12] and high triangularity (higher density) magnetic configurations. The more recent data added to that database are from discharges at high density, low edge safety factor and high triangularity. Figure 4 shows the figure of merit ($N^{GW} \times H_{98(y,2)}$) for the low triangularity discharges and the high triangularity discharges with nitrogen seeding and type-III ELMy edge. The high triangularity allows to operate at higher density without sacrifice in confinement. This has been first shown in deuterium seeded type-I ELMy H-modes [13, 14] and impurity seeded type-I ELMy H-modes [15]. This results in an increase of the product $N^{GW} \times H_{98(y,2)}$ by approximately 20%. No principle deterioration was found with the radiative power fraction. The confinement is similar in very strongly radiating plasmas with radiative power fractions close to 100% and in plasmas close to the type-I to type-III ELMy H mode transition at 64% radiative power fraction (see figure 5).

Figure 6 shows the confinement enhancement factor $H_{98(y,2)}$ as function of the collisionality. As can be seen in table 1, a large operational range is covered in this database. It also includes Hybrid discharges. There is no systematic difference between standard ELMy Hmodes and Hybrid discharges observed. The data set shows no apparent dependence of the confinement enhancement factor on collisionality. However, looking only at the high triangularity discharges at low edge safety factor leads to the suggestion that the confinement is slightly increasing towards lower collisionality. In figure 7 the confinement at collisionalities close to 0.1 is about $H_{98(y,2)} \approx 0.85$ in 3.25MA discharges.

In figure 8 the $H_{98(y,2)}$ is shown versus the normalized gyro radius. The operational do main covered at JET does extend from 0.9MA/ 1T AUG, CDH-mode [16] identity pulses up to 3MA with high and low q_{95}, as well as 2.5MA / 3.45T low * pulses with heating powers of up to 33MW. Within one plasma current and configuration the $H_{98(y,2)}$ does decrease with decreasing ρ^*. This is an effect of the increased gas fuelling in those experiments, which leads to lower pedestal as well as core temperatures. However, all those lines are parallel to each other. Comparing the data at high ρ^* with the 2.5MA/3.45T pulses leads to the conclusion that the confinement scales like $\rho^{*-2.5}$. However this could be due to a different β dependence in the $H_{98(y,2)}$ scaling [17]. Neglecting this would lead to a scaling, which is closer to gyro-Bohm scaling: $B\tau_{E-gyro-Bohm} \propto \rho^{*-}3.0$.

5. EDGE OPERATIONAL SPACE

Figure 9 shows the edge operational space of the high triangularity discharges with nitrogen seeding. The ion pedestal temperature is taken from Charge Exchange Spectroscopy and the pedestal electron density is taken from LIDAR. Figure 9 shows data for discharges from 2.5MA / 2.0T to 3.25MA / 2.6 T at a constant edge safety factor of $q_{95} = 2.6$. Remarkable is the strong increase in the electron

temperature. By lowering the collisionality the pedestal temperature was increased from 0.4keV to about 1.0keV in the high triangularity discharges (see figure 10). This has to be extrapolated to the 17 MA ITER $Q = 10$ scenario at $N^{GW} = 1$, for which a pedestal temperature of 2-2.5keV is necessary [18, 19]. In figure 10 the ITER value is shown together with the JET pedestal temperature data illustrating the gap in the data. Although global data for much lower collisionalities for nitrogen seeded type-III ELMy H-modes are available, those pulses lack of good pedestal data. The model proposed by Pogutse and Igitkhanov [18, 19] described reasonably well the edge operational space of unfuelled type-III ELMy H-mode at low collisionality [20]. In this model the type-III ELMs are described by an instability based on Resistive Interchange modes driven by magnetic Flutter (RIF). When the radial electric field just inside the separatrix becomes sufficiently strong, it can stabilize the RIF [20]. The model gives a critical pedestal temperature for the transition from type-III ELMs to type-I ELMs, which is different for high and low collisionality. For high collisionality the critical temperature is only weakly proportional to the magnetic field ($T_{0crit} \propto q_{95}^{24/17} B_t^{10/17}$), whereas for low collisionality the dependence on the magnetic field is stronger ($T_{0crit} \propto q_{95}^{18/5} B_t^{2}$). The data of the nitrogen seeded type-III ELMy H-modes shown in figure 9 lead to the conclusion that the dependence on the magnetic field is closer to B_t^{2}). As figure 10 shows, the collisionality varies by more than a factor of 3 from high collisionality to intermediate collisionality. This could be an explanation, why the critical temperature is increasing so strongly with the magnetic field. And this could also explain, why the confinement enhancement factor $H_{98(y,2)}$ is slightly increasing towards lower collisionality as figure 7 suggests. However, the model of Pogutse and Igitkhanov does not reflect the q_{95} dependence of the experiments [20]. Hence some uncertainties in the prediction of the type-I to type-III ELMy H-mode threshold remain.

Often the type-III ELMs are also associated with resistive ballooning instabilities. A model based on resistive ballooning instabilities was used to describe the type-I to type-III ELM back transition in strongly fuelled discharges [21]. Hence this model is based on the dimensionless pressure gradient and the collisionality. A critical density for the back transition to type-III ELMs can be derived: $n_{e,crit} \propto B_t \sqrt{f(s)}/(q_{95}^{5/4} R^{3/4} Z_{eff}^{1/4})$, with $f(s)$ being a function of the shear. This model reflects better the inverse q_{95} dependence on the back transition [20]. Both, the inverse q_{95} dependence and the inverse Z_{eff} dependence will be favourable for the proposed ITER scenario at 17MA and $N^{GW} = 1$. Hence, it should be possible to reach high pedestal densities in this regime too.

The evidence that at lower collisionalities the dependence of the critical temperature for the type-III to type-I ELM transition on the magnetic field is strong, leads to the suggestion that for ITER a higher pedestal temperature can be expected and hence higher pedestal pressure. A higher pedestal temperature would also result in a higher plasma core temperature assuming stiff temperature profiles. Altogether, this leads to positive predictions for ITER.

6. PROFILE PEAKING

All ITER simulations are based on a flat density profile. The confinement could be improved, if the

plasma core density could be increased above the value of the pedestal density. It is suggested that towards lower plasma collisionality the density is peaked in the plasma centre [22]. The experiments described in [22] are type-III ELMy H-modes without any additional gas fuelling, just fuelled by neutral beam injection. The strongly radiating type-III ELMy H-modes presented here have strong external gas fuelling by deuterium and nitrogen. Figures 11 and 12 show the electron density peaking as derived from LIDAR versus the collisionality and versus the normalized electron density. It is usually difficult to separate the effect of density from the effect of the collisionality due to it's co-linear behaviour [23]. However, careful analysis suggests the presence of an anomalous pinch leading to density peaking, which could increase the fusion power in ITER by almost 30% [23]. Figure 11 suggests a density peaking with decreasing collisionality, however figure 12 suggests that the density peaking is more related to the normalized density (and maybe underlying effects of core fuelling versus edge fuelling). A detailed transport study, including the effect of sources, has not been carried out here. However, it seems that the correlation between density peaking and normalized density is larger than the one with density peaking and collisionality. Explicitly the regressions yield: $n_e(0)/n_e(0.8) = 1.0784 - 0.0758 \ln \nu^*$ with $R^2 = 0.115$ and $ne(0)=n_e(0.8) = 1.5935 - 0.5287 N^{GW}$ with $R^2 = 0.4478$.

It should also be noted here that density peaking not only is favourable for fusion power, but might also to an increased impurity concentration in the plasma core. In particular high-Z elements tend to accumulate as a result of neo-classical transport in the plasma core, when the density profile is peaked. This accumulation of high-Z elements might even be amplified in impurity seeded discharges [24] due to impurity-impurity driven forces. The loss of sawtooth activity has then an absolute negative effect on the core plasma pollution.

7. PLASMA POLLUTION

The plasma pollution is a result of impurity production, plasma transport and radiation efficiency. Both impurity production and radiation efficiency are strongly dependent on the plasma density. Hence, the plasma pollution (Z_{eff}) depends strongly on the absolute density in those highly radiating plasmas. In recent JET campaigns the standard radiating type-III ELMy H-mode has been extended to higher plasma current (3.25MA) and therefore high absolute density. At those high densities the Z_{eff} is strongly reduced. The effective charge Z_{eff} was reduced from 2.2 to values below 1.5, mainly due to the increased absolute density and reduced carbon erosion. In those highly radiative discharges ($f_{rad} \geq 0.75$) nitrogen having replaced carbon, is the main radiator and the dominant impurity in the plasma.

The impurity production in the divertor is generally reduced towards higher density and higher radiative power fraction [6, 25]. A comparison of the carbon erosion in the divertor and the main chamber wall, revealed that the main chamber wall erosion is much lower in type-III ELMy H-modes, when compared to type-I ELMy H-modes [25]. This is also reflected in the hydrogen retention in the type-III ELMy H-modes, which is determined by the co-deposition of carbon and hydrogen in the inner divertor. The carbon transported to the inner divertor does have it's origin mainly in the

main chamber. The chemical erosion of carbon is enhanced by the chemical erosion through nitrogen. Detailed investigations are ongoing and will be reported in the future.

Furthermore, the divertor geometry and the fuelling location have an impact on the plasma pollution [26]. A closed divertor leads to a stronger detachment at similar electron densities when compared to an open divertor. Also fuelling close to the outer divertor strike point can reduce the plasma pollution [26]. However, full detachment can increase substantially the penetration depth of deuterium and impurity ions leading to a higher Z_{eff} in the plasma core. This increased penetration depth is a general behaviour in impurity seeded discharges (see also [27]).

Naturally, for the type-III ELMy hybrid mode the Z_{eff} is higher since the density is lower and the heating power is much higher. At a density of $\bar{n}_e = 7\times10^{19}$ m^{-3} the Z_{eff} is about 3. On basis of an enlarged database a new Z_{eff} scaling has been developed [25]: $Z_{eff} = 1 + 40P_{rad}Z^{0.12}\tau_E S^{-0.94} n_e^{-1.5} a_{min}^{-1} R^{-1}$, with S being the plasma surface, *amin* the minor radius and R the major radius. The main improvement of this scaling is the introduction of the impurity transport. This has already been done successfully for other tokamaks [28]. For the high density 17MA scenario with a fusion power of 400MW and a $H_{98(y,2)} = 0.75$, at a density of $N^{GW} = 1$ a Z_{eff} of 1.9 is predicted, excluding any contribution from Helium. This is above the assumptions made for ITER, which include Helium. However, details of the radial impurity transport and profile effects in the temperature and density profiles are not taken into account. For the standard 15 MA ITER scenario with $H_{98(y,2)} = 1$ and a density of $N^{GW} = 0.85$ the $Z^{eff} = 2.5$ is worse. A review of the tokamak size dependence is necessary though, to reduce error bars in this prediction.

8. MHD STABILITY

All ELMy H-modes at JET are marginal unstable to the development of neoclassical tearing modes (NTMs) [29]. The radiative scenarios are particularly prone to NTMs, because of its dependence of the marginal beta $\bar{}Nmarg$ on the normalized poloidal ion gyroradius $\rho^*_{p.i} = \rho_{p.i} / a_{min}$ [30], which is low in the radiative scenarios with the cooled pedestal. Seed islands produced by large sawtooth crashes can trigger the NTMs, when β_N is larger than the critical marginal β_{Nmarg} [29]. The disturbance and hence the seed island is particular large in sawtooth crashes where a large volume is affected, hence large sawtooth inversion radius. Operation at $q_{95} = 2.6$ has the disadvantage of having a large sawtooth inversion radius (figure 13), which potentially leads to larger sawtooth crashes. A scenario had to be developed to avoid triggering the NTMs ($m/n = 3/2$) in the transient period of the ramp up in the radiative scenario, where the sawtooth period is the longest. Setting $q_{95} = 3.4$ at the beginning of the heating period and ramping down to $q_{95} = 2.6$, once regular sawtooth activity is obtained, is the major recipe to avoid NTMs. During the flat top period of the highly radiative scenario, sawtooth activity is benign. In particular at the high plasma densities, which are an integral part of the highly radiative type-III ELMy H-mode, the relative sawtooth amplitude is small (see figure 14). To prevent any impurity accumulation in the plasma core ICRH is added with a heating power of 1-3MW. This is a typical method to maintain sawtooth activity in impurity seeded discharges [31].

However, also large ELMs can trigger NTMs. To avoid large ELMs a minimum gas fuelling is necessary throughout the heating power phase to avoid large ELMs and keep the ELM frequency at a level above 20Hz. Figure 15 a comparison of two plasma pulses with different gas fuelling recipes is shown. In the Pulse No: 74344 the gas fuelling of both, deuterium and nitrogen, is too low and hence the ELM frequency is below 20Hz. This triggers a 3/2 NTM at 15.413s as can be seen in the detailed figure 16 by the growth of the n=2 activity. When the gas fuelling is increased by almost a factor of 2 the ELM frequency is increased sufficiently to avoid triggering of ELMs.

The MHD activity observed during the hybrid type-III ELM operation is characterized by mild n=1 sawteeth precursors present during the high β_N and n=3 mode presents near the q = 4/3 surface [32]. The more deleterious 2/1 and 3/2 NTM are not present during the hybrid type-III ELM case and nor in the reference type-I case. The core q-profile of the integrated hybrid type III ELM is very similar to the q-profile of the reference hybrid type I ELM scenario 17, indicating that type III ELM operation obtained with N-injection is compatible with high N operation with minimized impact of sawteeth on the stability.

9. EXTRAPOLATION TO ITER WITH THE INTEGRATED MODEL COREDIV

The nitrogen seeded high triangularity JET discharges have been modelled with COREDIV [33]. COREDIV is an integrated model solving self-consistently the 1D energy and particle transport of plasma and impurities in the core region and 2D multifluid transport in the SOL [34]. The energy confinement is scaled with the empirical $H_{98(y,2)}$ scaling. The target erosion by nitrogen is not included. The carbon target erosion is dominated by deuterium and self sputtering. The chemical erosion yield is calculated according to the flux dependence given in [35]. No main chamber erosion was included in the calculations. However, the experimental data (main plasma profiles in the core, the radiated power and the plasma pollution) were reconstructed satisfactory. On the basis of this benchmarking to JET experiments predictions for ITER were done. In the ITER case neon was seeded as radiating impurity. The target was again a carbon target. Figure 5 shows the results of the COREDIV simulations for the 15MA standard ITER scenario for a set of densities and confinement enhancement factors. The results indicate, with reasonable accuracy, that this plasma scenario can achieve a powe amplification factor Q in excess of 6 at 15MA (q_{95} = 3.0) with auxiliary heating powers of 40MW. Higher heating power will have a detrimental effect on the fusion amplification factor. However, as reported above, a slight increase in confinement towards lower collisionality might be possible due to an increased pedestal temperature or density peaking. With an $H_{98(y,2)}$ = 0.85 and N^{GW} = 1 a fusion power amplification of close to 10 should be possible with 15MA operation. For 17MA (q^{95} = 2.6) the extrapolations with the code show the compatibility of those strongly radiating type-III ELMy H-modes with a power amplification in excess of 10 (see figure 8). In both cases, 15MA and 17MA, the plasma core pollution is below Z_{eff} = 1.5 (see figure 9 and 10). This does not include any contribution from the Be-wall. Assuming a core concentration of 2% of Be in the plasma core would then increase the Z_{eff} to about 1.7, consistent with former ITER predictions [4].

SUMMARY AND CONCLUSION

A large data base on radiative type-III ELMy H-mode at JET does allow a reasonable extrapolation to ITER. Within the error bars of the data and based on the simplicity of the extrapolation models the extrapolation to ITER does allow the following statements: (a) the confinement (transport) should be sufficient to reach $Q = 10$ at 17MA depending on point d; (b) the steady state heat load will be reduced to acceptable values; (c) the transient heat load should be acceptable even with respect to the most stringent limits; (d) the plasma pollution and hence the plasma core dilution could be slightly to high, leading to some reduction in plasma performance; (e) the accessibility of the type-III ELMy regime at higher pedestal temperatures seems to be possible; operation at low q_{95} seems to be possible and reliable. It seems that the operation at low collisionality leads to slightly increased confinement, likely due to an increased pedestal temperature. With some uncertainties in the predictions and extrapolations operation at 15MA might be possible with fusion amplification factors close to 10.

If the confinement time of future ITER hybrid discharges (presently foreseen at low plasma current Ip 14MA) is high enough to allow type-III ELMy operation with acceptable fusion performance ($Q \geq 5$), then the experimental procedure described here can be envisaged to control the edge plasma conditions and get sustainable heat load (compatible with the ITER walls) without modifying the core q-profile, and thus the high N capability of the hybrid scenario (optimized for current drive sources and non-inductive current bootstrap). The relatively high impurity content and the extrapolation to ITER remain important issues to demonstrate the viability of the hybrid type-III ELM scenario as an integrated scenario for ITER. The use of the real-time control, maximization of confinement as observed in ASDEX Upgrade [36] and impurity decontamination techniques will be essential to improve the performances and the reliability of the scenario.

ACKNOWLEDGEMENTS

This work, supported by the European Communities under the contract of Assocation between EURATOM/FZJ, was carried out within the framework of the European Fusion Development Agreement. The views and opinions expressed herein do not necessarily reflect those of the European Commission.

REFERENCES

[1]. Lowry C, PWI EU Task Force Meeting (29-31 October 2007, Madrid, Spain)
[2]. Zohm H *et al* 1996 Plasma Physics and Controlled Fusion **38** 105
[3]. Wagner F *et al* 1982 Physics Review Letters **19** 1408
[4]. Shimada M, *et al* , 2000 J. Plasma Fusion Res. Ser. **3**, 77
[5]. Greenwald M *et al* 1988 Nuclear Fusion **28** 2199
[6]. Rapp J, *et al* , 2005 Jornal of Nuclear Materials **337-339**, 826
[7]. Joffrin E, *et al* , 2005 Nuclear Fusion **45**, 626
[8]. Rapp J, *et al* , 2002 Plasma Physics and Controlled Fusion **44**, 639
[9]. Rapp J, *et al* , 2004 Nuclear Fusion **44**, 312

[10]. Eich T, *et al* , 2008 Proceedings of the 18th International Conference on Plasma Surface Interactions (26-30 May 2008, Toledo, Spain)
[11]. Cordey J.G, *et al* , 2002 Plasma Physics and Controlled Fusion **44**, 1929
[12]. Matthews G.F *et al* 1999 Nuclear Fusion **39**, 19
[13]. Lomas P.J *et al* 2000 Plasma Physics and Controlled Fusion **42**, B115
[14]. Saibene G *et al* 2002 Plasma Physics and Controlled Fusion **44**,1769
[15]. Dumortier P *et al* 2002 Plasma Physics and Controlled Fusion **44**, 1845
[16]. Kallenbach A *et al* 1995 Nuclear Fusion **35**, 1231
[17]. Cordey J.G, *et al* , 2005 Nuclear Fusion **45**, 1078
[18]. Igitkhanov Yu, *et al* , 1998 Plasma Phys. Control. Fusion **40**, 837
[19]. Igitkhanov Yu, *et al* , 2000 Contrib. Plasma Phys. **368**
[20]. Sartori R, *et al* , 2004 Plasma Physics and Controlled Fusion **723**
[21]. Chankin A.V. and Saibene G. 1999 Plasma Physics and Controlled Fusion **41**, 913
[22]. Valovic M, *et al* , 2004 Plasma Physics and Controlled Fusion **46**, 1877
[23]. Weisen H, *et al* , 2006 Plasma Physics and Controlled Fusion 48, A457
[24]. Rapp J, *et al* , 1997 Plasma Physics and Controlled Fusion **39**, 1615
[25]. Rapp J, *et al* , 2009 accepted for publication in Jornal of Nuclear Materials
[26]. Rapp J, *et al* , 2008 Plasma Physics and Controlled Fusion **50**, 095015
[27]. Unterberg B, *et al* , 1997 Plasma Physics and Controlled Fusion **39**, B189
[28]. Telesca G, *et al* 1997 Jornal of Nuclear Materials **241-243**, 853
[29]. Sauter O, *et al* , 2002 Physical Review Letter **88**, 105001
[30]. Koslowski H.R., *et al* , 2000 Nucl. Fusion **40**, 821
[31]. Nave M.F.F, *et al* , 2003 Nuclear Fusion **43**, 1204
[32]. Corre Y, *et al* , 2008 Plasma Physics and Controlled Fusion **50**
[33]. Zagorski R, Telesca G and Rapp J 2008 Contrib. Plasma Phys. 179
[34]. Zagorski R and Stankiewicz R, 2003 Jornal of Nuclear Materials **313-316**, 899
[35]. Roth J, *et al* , 2004 Nuclear Fusion **44**, L21
[36]. Sips A.C.C, *et al* , 2002 Plasma Physics and Controlled Fusion **44**, A151

Parameter	***Range***
I_P	0.95-3.25MA
B_t	1.0-3.45T
q_{95}	2.3-4.3
δ	0.18-0.47
N^{GW}	0.4-1.0
β_N	0.9-2.6
P_{heat}	2.3-33MW

Table 1. Operational range of type-III ELMy H-modes with nitrogen seeding.

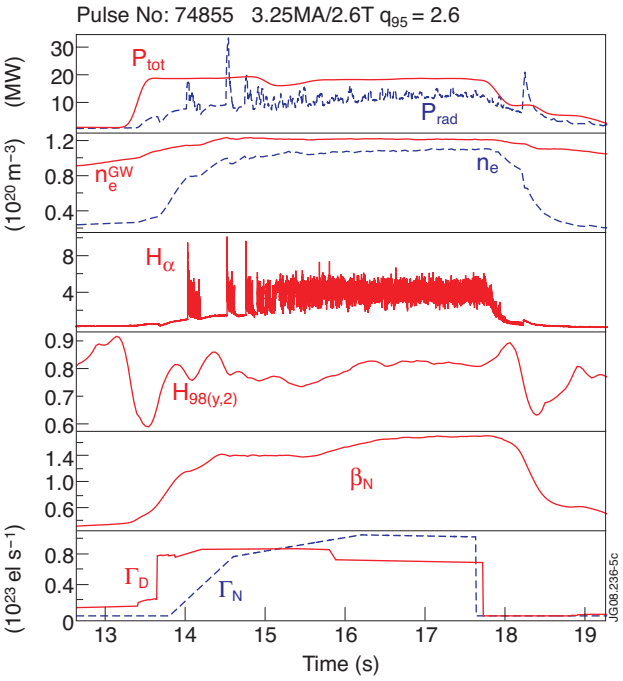

Figure 1: Overview of 3.25MA/2.6T type-III ELMy H-modes at JET (Pulse No: 74855).

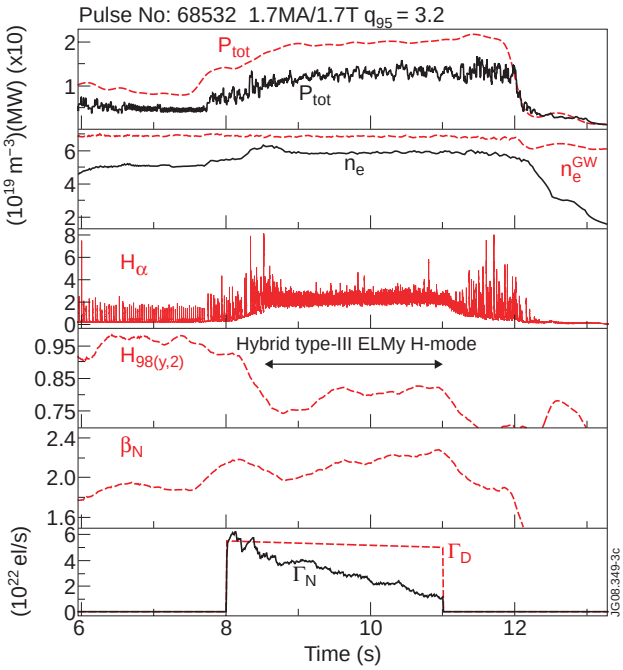

Figure 2: Overview of a 1.7MA/1.7T type-III Hybrid discharge at JET (Pulse No: 68515).

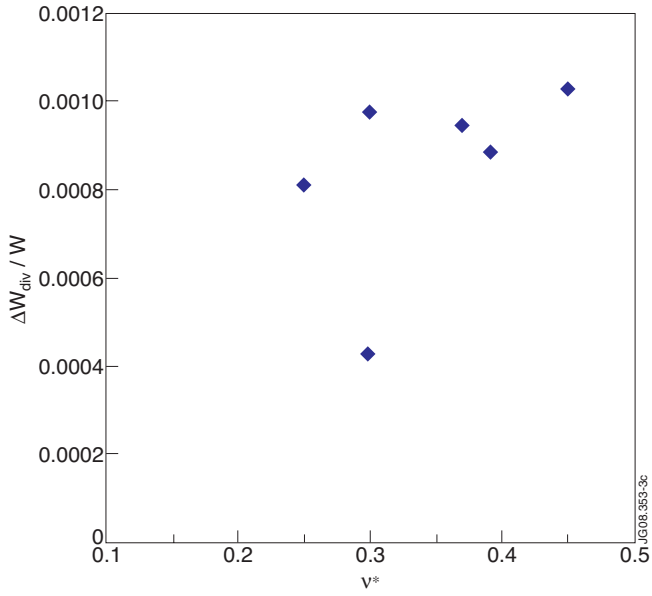

Figure 3: ΔW=W as a function of collisionality as derived from IR thermography for 2.5MA/2.0T type-III ELMy H-modes at JET.

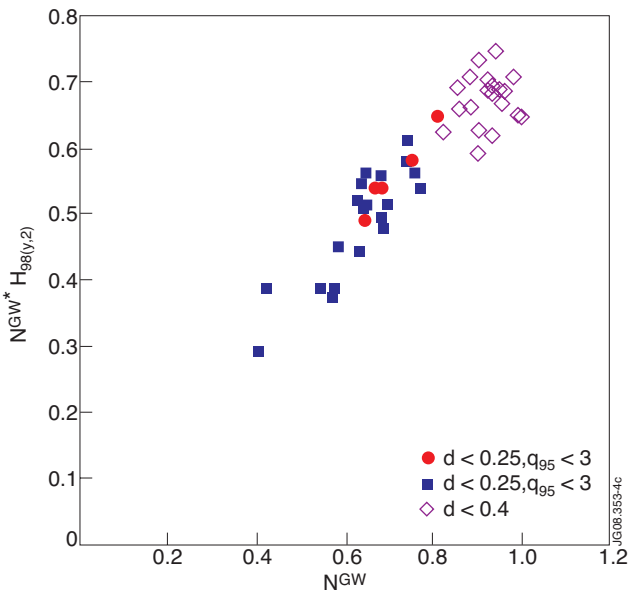

Figure 4: The product of $N^{GW} \times H_{98(y,2)}$ as a function of normalized density N^{GW} for radiative type-III ELMy H-modes.

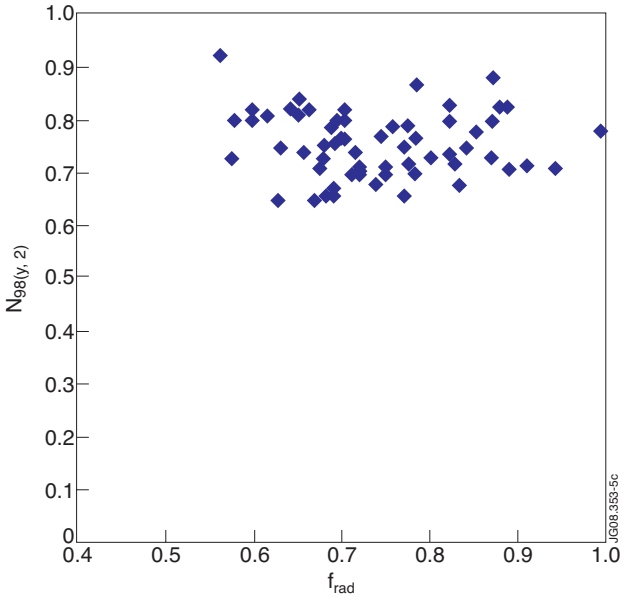

Figure 5: $H_{98(y,2)}$ as a function of the radiative power fraction for type-III ELMy H-modes with nitrogen seeding.

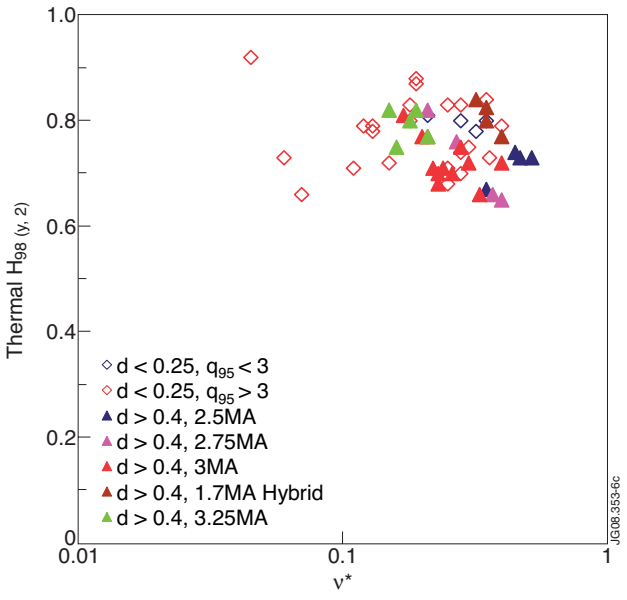

Figure 6: $H_{98(y,2)}$ as a function of collisionality for radiative type-III ELMy H-modes at JET.

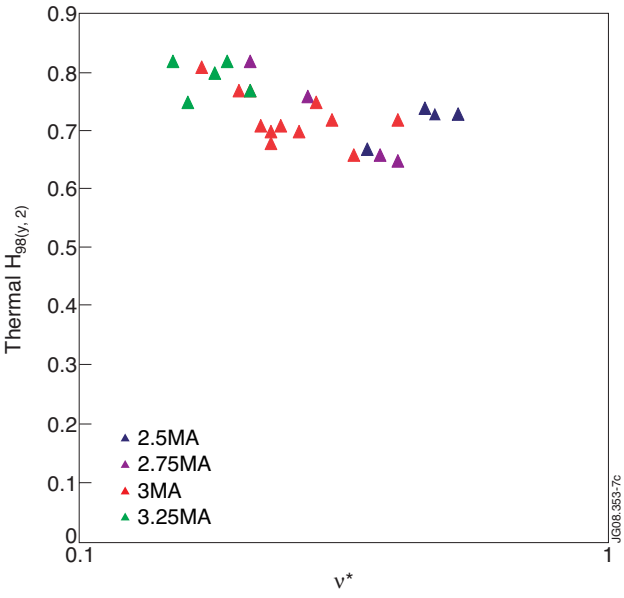

Figure 7: $H_{98(y,2)}$ as a function of collisionality for radiative type-III ELMy H-modes in high triangularity configurations and low q_{95} scenario at JET.

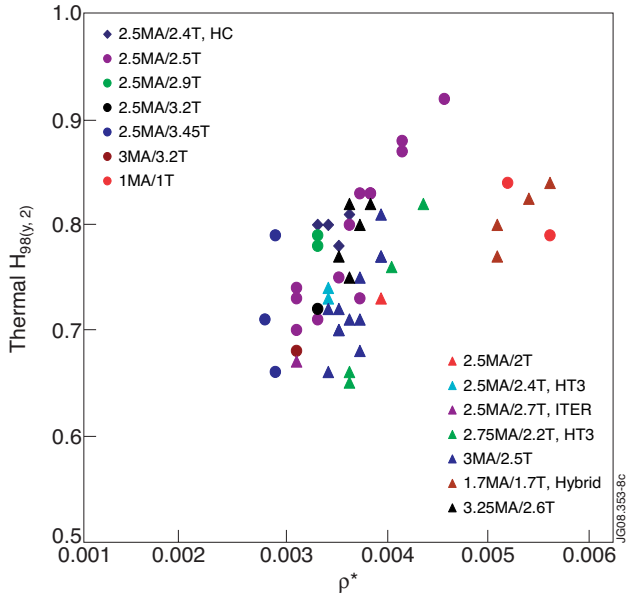

Figure 8: $H_{98(y,2)}$ as a function of normalized gyro radius for radiative type-III ELMy Hmodes at JET.

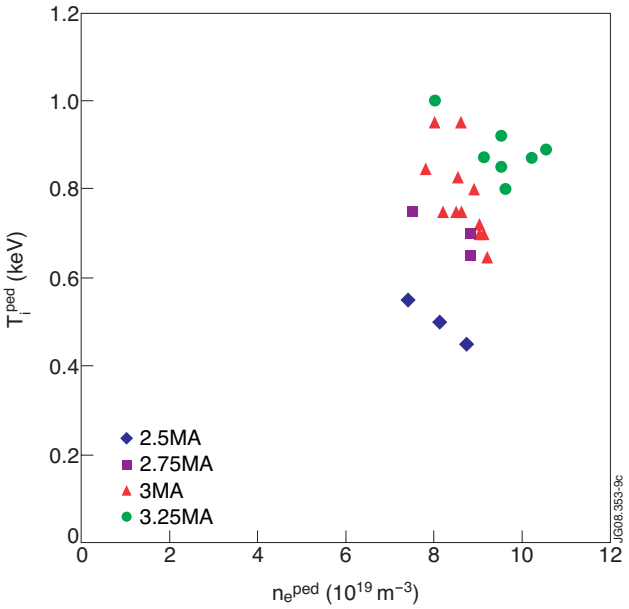

Figure 9: Pedestal ion temperature as a function of the pedestal electron density for radiative type-III ELMy H-modes at JET

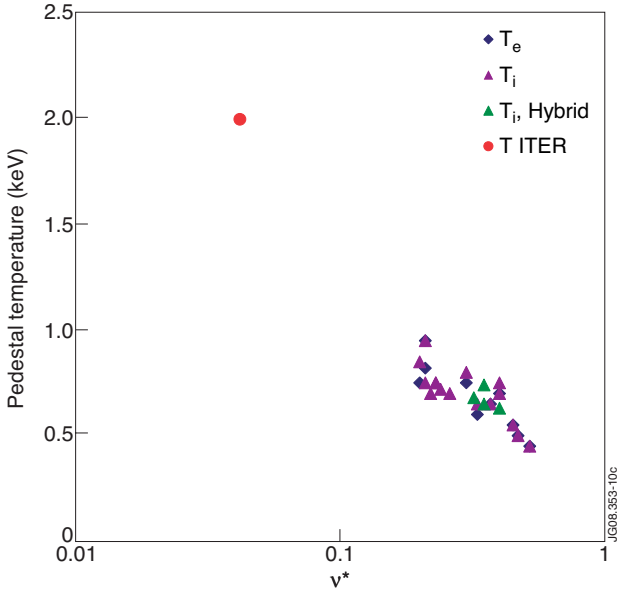

Figure 10: Pedestal temperature as a function of collisionality for radiative type-III ELMy H-modes at JET

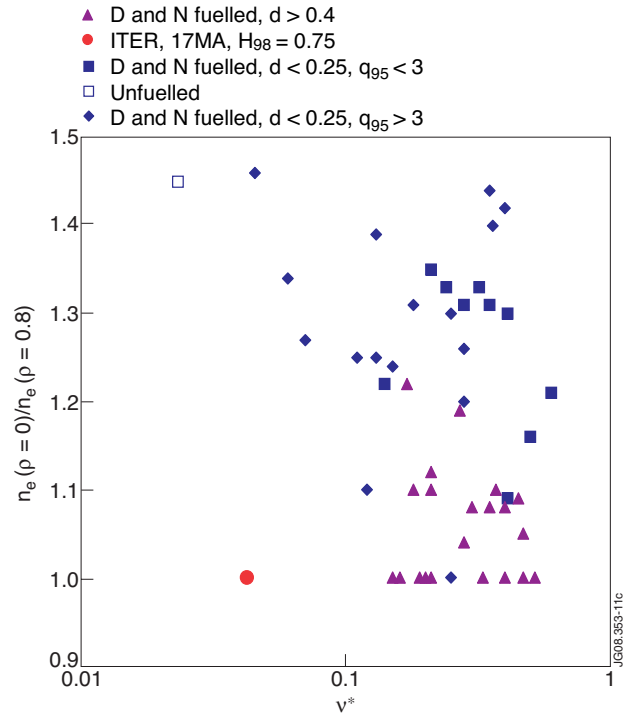

Figure 11: Peaking of the electron density profile versus collisionality for radiative type-III ELMy H-modes at JET.

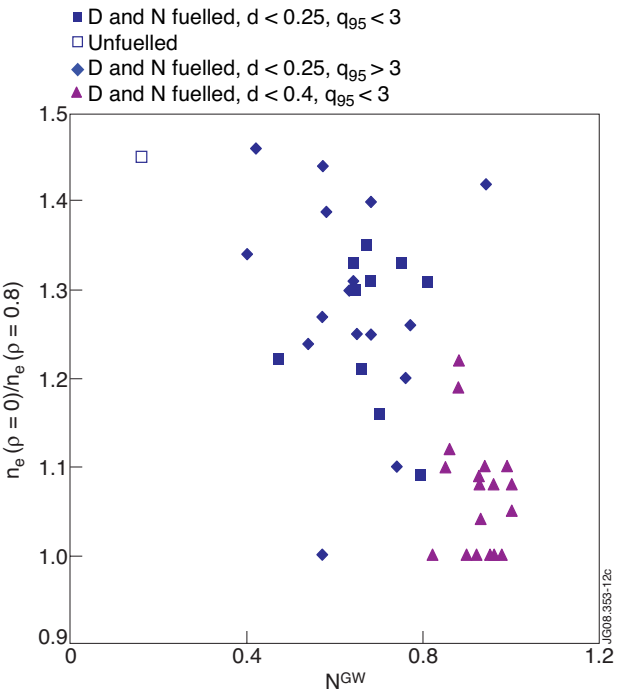

Figure 12: Peaking of the electron density profile versus the normalized gyro radius for radiative type-III ELMy H-modes at JET.

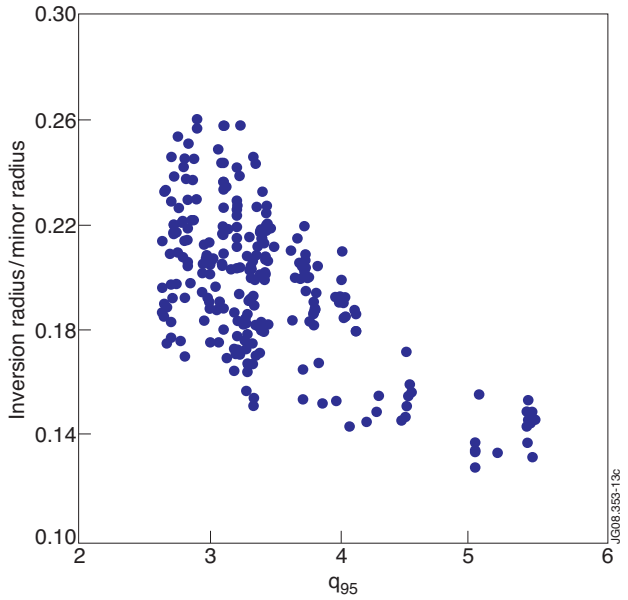

Figure 13: Sawtooth inversion radius normalized to minor radius versus q_{95} for JET NBI heated plasmas (with deuterium fuelling).

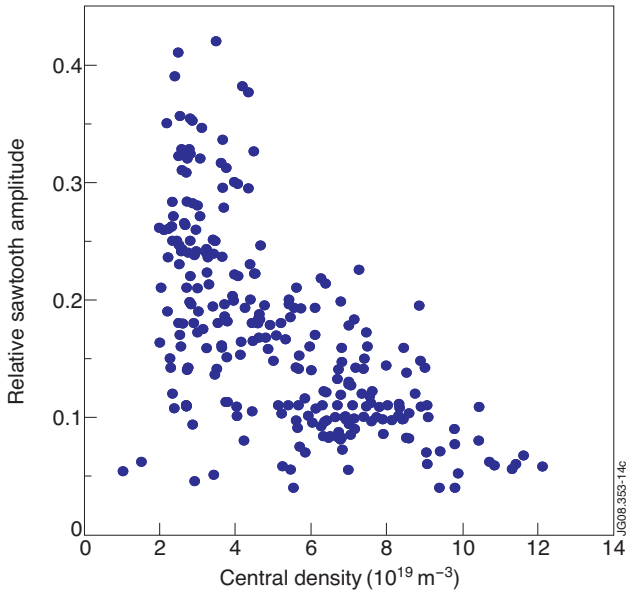

Figure 14: Relative sawtooth amplitude versus central density for JET NBI heated plasmas (with deuterium fuelling).

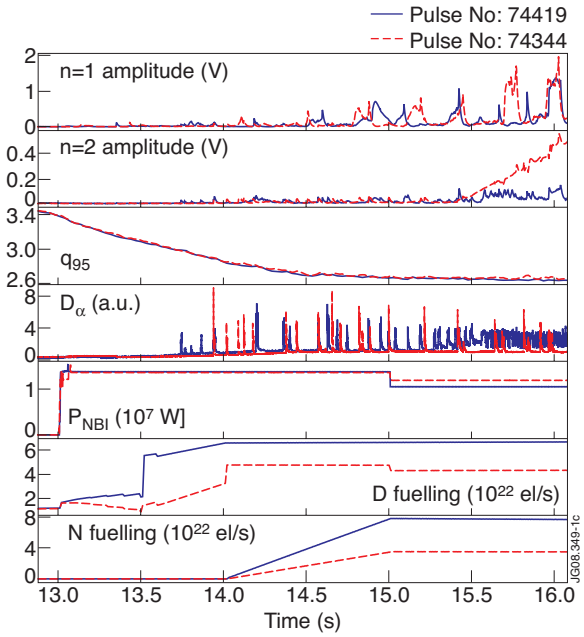

Figure 15: Comparison of two plasma pulses with different fuelling; n=1 MHD activity, n=2 MHD activity, q_{95}, H_α light in divertor, neutral beam power, deuterium gas fuelling rate, nitrogen gas fuelling rate: Pulse No: 74344 develops a 3/2 NTM; Pulse No: 74410 does not develop any NTM.

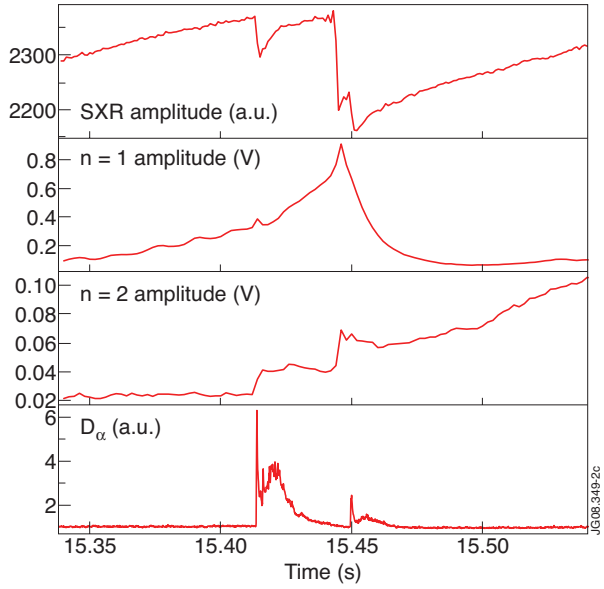

Figure 16: NTM onset due to ELM; Soft X Ray amplitute of central line-integrated signal, n=1 MHD activity, n=2 MHD activity, H_α light in divertor: ELM at 15.413s triggers n=2 activity (3/2 NTM); Sawtooth crash at 15.45s.

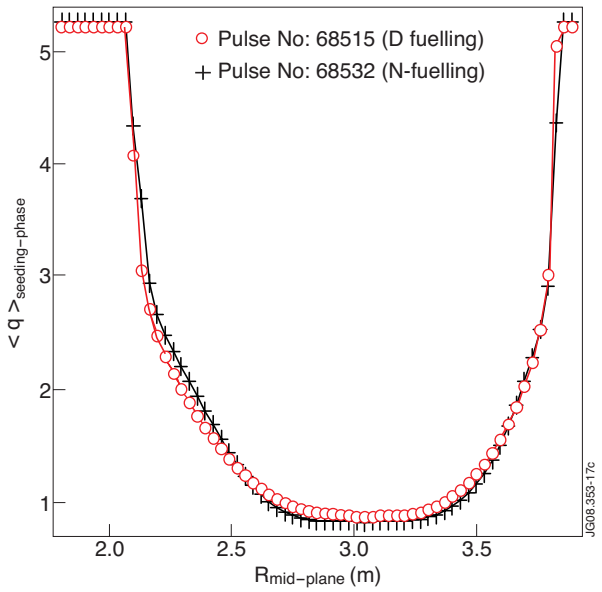

Figure 17: Time average of q-profiles measured by the MSE system during the seeded phase t=[8-11s] for the pulse with D fuelling with type-I ELMs (crosses) and D+N fuelling with type-III ELMs (circles). Figure courtesy from [32].

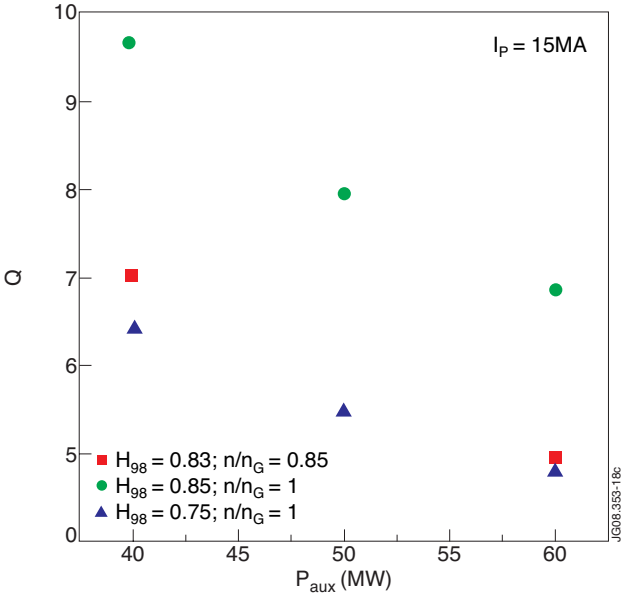

Figure 18: COREDIV: Fusion amplification factor Q versus the auxiliary heating power for the ITER 15MA scenario for radiative scenarios with neon seeding.

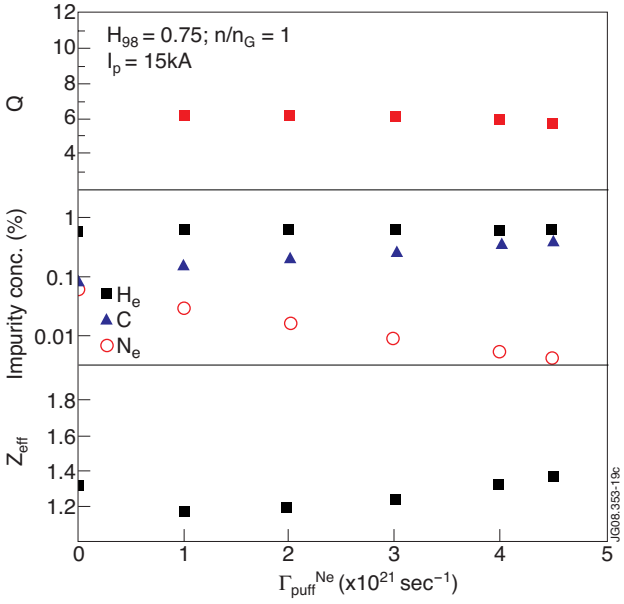

Figure 19. COREDIV: Fusion amplification factor Q, impurity concentration in the core plasma and Z_{eff} versus the neon gas fuelling rate for ITER 15MA scenario.

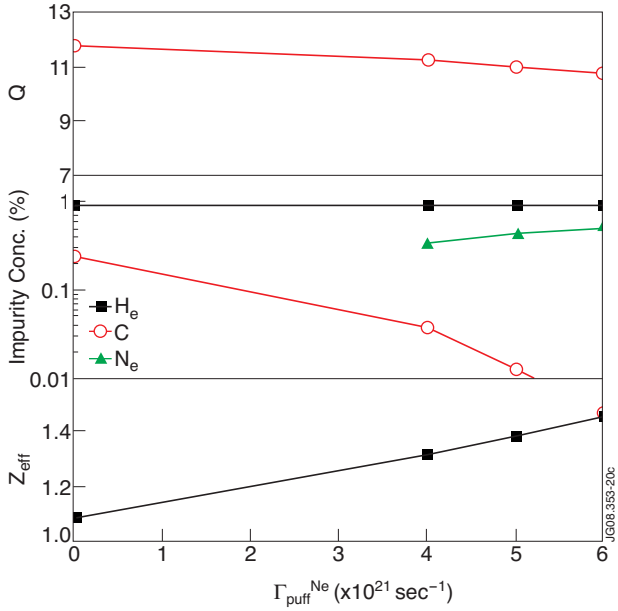

Figure 20. COREDIV: Fusion amplification factor Q, impurity concentration in the core plasma and Z_{eff} versus the neon gas fuelling rate for ITER 17MA scenario. Figure courtesy from [33].